energies

MDPI

Article

Reference Model Adaptive Control Scheme on PMVG-Based WECS for MPPT under a Real Wind Speed

Anto Anbarasu Yesudhas, Young Hoon Joo * and Seong Ryong Lee

School of IT Information and Control Engineering, Kunsan National University, 588 Daehak-ro, Gunsan-si 54150, Jeonbuk, Korea; yanbarasu94@gmail.com (A.A.Y.); srlee@kunsan.ac.kr (S.R.L.)
* Correspondence: yhjoo@kunsan.ac.kr

Abstract: Over the last few years, improving power extraction from the wind energy conversion system (WECS) under varying wind speeds has become a complex task. The current study presents the optimum maximum power point tracking (MPPT) control approach integrated with neural network (NN)-based rotor speed control and pitch angle control to extract the maximum power from the WECS. So, this study presents a reference model adaptive control (RMAC) for a direct-drive (DD) permanent magnet vernier generator (PMVG)-based WECS under real wind speed conditions. Initially, the RMAC-based rotor speed tracking control is presented with adaptive terms, which tracks a reference model that guarantees the expected exponential decay of rotor speed error trajectory. Then, to reduce the wind speed measurement errors, a recurrent neural network (RNN)-based training model is presented. Moreover, the asymptotic stability of the proposed control method is mathematically proven by Lyapunov theory. In addition, the pitch angle control is presented to efficiently operate the rotor speed within the allowable operating range. Eventually, the proposed control system demonstrates its effectiveness through simulation and experimentation using a prototype of 5 kW DD PMVG-based WECS. After that, the comparative results affirm the superiority of the proposed control method over existing control methods.

Keywords: permanent magnet vernier generator; variable speed wind turbine; reference model adaptive control

Citation: Yesudhas, A.A.; Joo, Y.H.; Lee, S.R. Reference Model Adaptive Control Scheme on PMVG-Based WECS for MPPT under a Real Wind Speed. *Energies* **2022**, *15*, 3091. https://doi.org/10.3390/en15093091

Academic Editor: Andrés Elías Feijóo Lorenzo

Received: 11 March 2022
Accepted: 21 April 2022
Published: 23 April 2022

1. Introduction

As the global demand for wind energy has grown, the amount of energy produced by wind turbine (WT) capacity has increased to gigawatts [1,2]. This demands the installation of larger generators capable of managing high torques and converting the vast majority of the energy collected by turbine blades. Consequently, it is not easy to handle both the volumetric size and total mass of the generator. Moreover, it should concern the material cost, the maximum weight support by the tower, and its vibration handling capability [3]. Therefore, the direct-drive (DD) permanent magnet synchronous generator (PMSG) without gears is being used to overcome these challenges. However, in this instance, the generator's weight and size become too heavy, proportionally increasing the nacelle's weight [4]. Hence, a low weight DD generator with a substantially greater power density is required to overcome all of the problems at once. In this regard, permanent magnet vernier generators (PMVGs) have gained much interest in wind energy conversion systems (WECSs) because they can generate higher torque density even in low-speed conditions due to their magnetic gear effect compared to PMSG. Furthermore, it has a significantly greater output power density since it employs the primary permanent magnet flux as the modulation flux simultaneously [5–7].

From this point of view, the DD PMVG-based WECS has been designed and discussed in [8]. This design method decreases the uncertainty and avoids the complexity of repetitive design and performance computations. The authors in [9] have investigated the PMVGs

in a small-scale uncontrolled passive wind energy system. As a result, they found that the inherently high internal reactance is advantageous for this application. Moreover, the authors in [10] have completed a comparative analysis of the performance and cost of the conventional and PMVG-based WECS. Based on this analysis, PMVG seems to be the most acceptable alternative to conventional generators in terms of power matching, torque quality and generator mass. In addition, a limited study focused on the design of efficient control and nonlinear modelling of the PMVG-based WECS. Therefore, this study deals with the nonlinear modelling and efficient tracking control design for the PMVG-based WECS under various wind conditions.

The maximum power point tracking (MPPT) controllers have been developed to increase the maximum power extraction (MPE) capability of the variable-speed WT generators under various wind conditions [11]. It can be divided into two methods: pitch angle regulation and rotor speed regulation-based MPPT control techniques. In this regard, the authors establish various MPPT methods for maximizing wind power, such as linear quadratic Gaussian (LQG) control [12], sliding mode control [13,14], fuzzy control [15] and optimal power curve estimation algorithm [16]. Even so, these techniques have significant disadvantages, including the lack of ability to follow references and reject system disturbance. Furthermore, the authors in [17] have introduced the polynomial disturbance observer-based MPPT control techniques for WECS, which can determine the aerodynamic torque, wind speed and electromagnetic torque without sensors. However, this approach has high computational complexity. Similarly, an adaptive hybrid intelligent MPPT control was investigated in [18] to approximate the effective wind speed and the optimal rotor speed of variable-speed wind turbines. The authors in [19] have proposed an adaptive perturbation and observation approach-based MPPT scheme for PMSG-based WECS, in which step size is proportional to the slope, and it enhances the tracking capability. However, constantly changing wind conditions can cause the step size to be larger, affecting the tracking performance. Unlike the previously described MPPT methods, the proposed method can significantly improve the dynamic performance of the PMVG-based WECS to achieve an MPE from the varying wind speed conditions.

On the other hand, neural networks (NN) have advantages in universal approximation, quick learning capabilities, parallel computing, and fault tolerance [20]. Thus, the NN-based MPPT control algorithms are most popular in the WECS [21]. From this perspective, the authors in [22] have been presented a robust control technique by combining MPPT and pitch angle control for variable-speed WT systems. In this approach, the artificial NN adjusts the pitch angle to select the optimum generator speed for stable power extraction. In addition, the authors in [23] investigated the MPE approach using a cascade forward NN. This method presented the multi-layer cascade forward backpropagation technique rather than the most basic and widely used feed-forward multi-layer perceptron scheme. Following that, the authors in [24] have introduced a self-recurrent wavelet NN control approach for WECS and it has local self-feedback loops in a self-recurrent wavelet neural network, which give the memory function and the essential knowledge of historical signal values. The authors in [25] have proposed an upgraded gray BP NN and a modified ensemble empirical mode decomposition auto-regressive integrated moving average for real-time wind speed estimation. However, the aforementioned control algorithms are dependent on the wind measuring sensors, and it takes much time to collect the wind data. In the case of faulty wind sensors, the estimation methods results can be inaccurate. To handle this issue, in this study, a recurrent neural network (RNN) is presented to estimate wind speed without using wind speed measurement sensors. Moreover, the RNN is well-suited for real-time control and identification applications for WECS.

In recent years, regulating a WECS under fluctuating wind speed and enhancing the quality of the electricity supplied to the grid has become a complex challenge. In addition, a limited study only focused on the design of efficient control of the PMVG-based WECS. Therefore, this study deals with the nonlinear modeling and efficient tracking control design for the PMVG-based WECS. The main contribution of this study is to present an

effective rotor speed tracking control and to estimate wind speeds even at varying wind speeds using RNN. The RNN eliminates the wind speed measuring sensors because it estimates the wind speed from the current data of the torque and the rotor speed. As a result, MPPT ensures the MPE capability and significantly improves the electrical efficiency of the WECS. The contributions of this study can be summarized as follows:

- First, the RMAC is proposed for DD variable-speed PMVG-based WECS, which tracks a reference model that guarantees the expected exponential decay of rotor speed error trajectory.
- Based on the given reference model, the proposed technique can ensure a rapid exponential decrease of the speed error trajectory. Moreover, to enhance the tracking capability of the proposed RMAC method, an adaptive compensative term and a stabilizing feedback control term are presented.
- A RNN is trained offline to learn the rotor speed and torque information. Then, the trained RNN-model is deployed online to retrieve the wind speed without using an additional wind speed sensor. Furthermore, the pitch angle adjustment is presented to maintain the optimum rotor speed under varying wind conditions.
- Finally, the proposed control system demonstrates its effectiveness through simulation and experimentation using a prototype of 5 kW DD PMVG-based WECS. Then, the comparative results validate the superiority of the proposed control over existing control methods.

The paper is organized as follows: The WT and PMVG dynamics are presented in Section 2. The design of RMAC and stability analysis are detailed in Section 3, and the NN and pitch angle controller is explained in Sections 4 and 5. Simulation and experimental results and their discussions are carried out in Section 6. Finally, Section 7 summarizes the conclusion.

2. Modeling of PMVG-Based WECS

This section provides an overview of the wind energy conversion system. It consists of the wind turbine and PMVG modeling. The topology of a DD PMVG-based WECS with basic architecture and control approaches are shown in Figure 1.

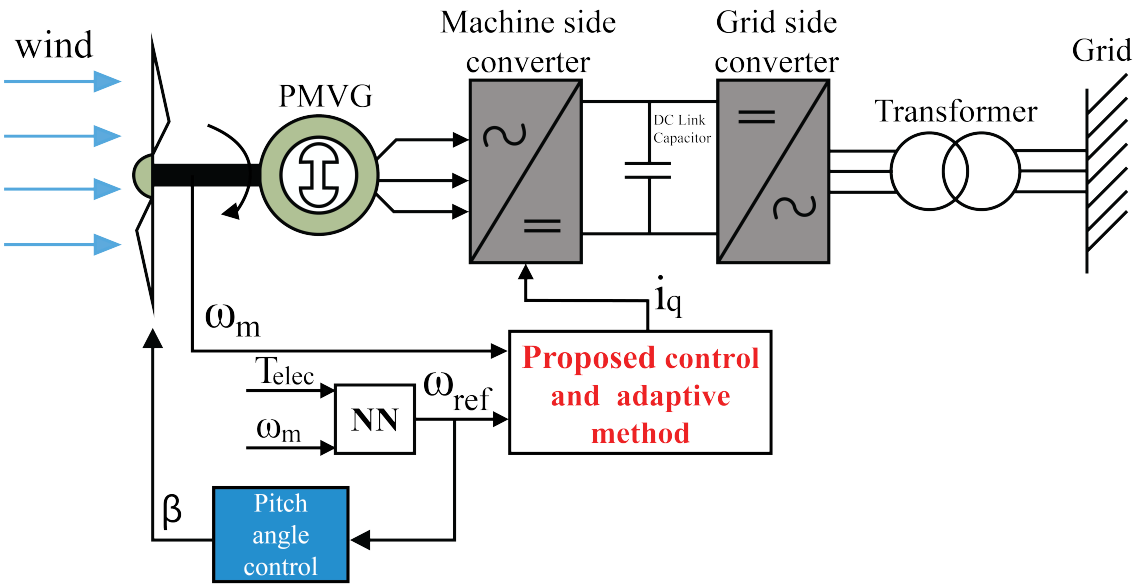

Figure 1. Basic topology of PMVG-based WECS with control strategy.

2.1. Wind Turbine Modeling

The amount of power generated by the WT is given by [8]:

$$P = \frac{1}{2}\rho A V^3 C_p(\lambda, \beta), \tag{1}$$

where ρ is the air density, V is the wind speed and $A = \pi R^2$ is the blade rotor swept area. Here, R is the radius of the WT blade. The power coefficient C_p is a function of the blade pitch angle β and tip speed ratio (TSR) λ.

$$\lambda = \frac{\omega_m R}{V}. \tag{2}$$

Here, the mechanical angular speed of a turbine is denoted by ω_m. With a changeable pitch angle β, the power coefficient $C_p(\lambda, \beta)$ of the WT can be defined as follows [26]:

$$C_p(\lambda, \beta) = 0.73\left(\frac{151}{\lambda_j} - 0.5\beta - 0.002\beta^{2.14} - 13.2\right)e^{-\frac{18.4}{\lambda_j}}, \tag{3}$$

λ_j is given as

$$\frac{1}{\lambda_j} = \frac{1}{\lambda - 0.02\beta} - \frac{0.003}{\beta^3 + 1}.$$

In general, there is an ideal TSR for each WT blade pitch angle β; it is indicated by $\lambda_{opt}^{\beta=0} = 6.912$. The maximum power coefficient $C_{p_{max}} = 0.441$ is obtained from the ideal TSR-based MPPT, which typically captures maximum power of 5 kW at various wind speeds. As shown in Figure 2 the cut-in, rated, and cut-out speeds are 3 m/s, 9 m/s, and 15 m/s, respectively. In addition, Figure 3 shows the typical power curve used in this study, which was obtained from (1).

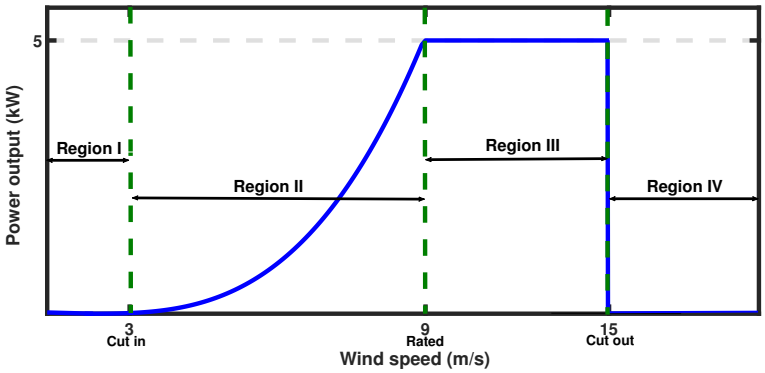

Figure 2. Different operating region of the PMVG-based WECS.

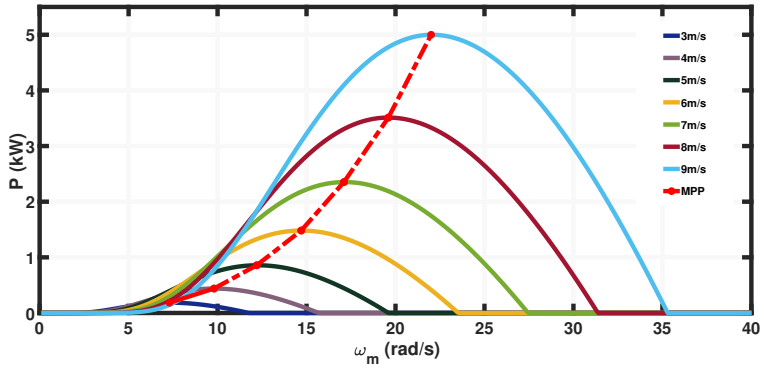

Figure 3. The wind power versus wind speed characteristics of the 5 kW PMVG-based WECS.

2.2. PMVG Modeling

Dynamic modeling of the PMVG can be described in the synchronously rotating $d-q$ reference system as follows [27]:

$$\begin{cases} V_{sd} = & R_s i_{sd} - \omega_s L_{sq} i_{sq} + L_{sd} \dfrac{di_{sd}}{dt}, \\ V_{sq} = & R_s i_{sq} + \omega_s L_{sd} i_{sd} + L_{sq} \dfrac{di_{sq}}{dt} + \omega_s \Phi_{mag}, \\ \dot{\omega}_m = & \dfrac{1}{J}\left[T_L - T_{elec} - B\omega_m\right]. \end{cases} \tag{4}$$

where V_{sd} and V_{sq} represent the $d-q$ frame stator voltages, R_s represents the winding resistance of the stator, and i_{sd} and i_{sq} represent the $d-q$ frame stator currents. The electrical rotating speed of the generator ω_s is the product of the generator pole pair P_n and the mechanical angular speed ω_m. L_{sd} and L_{sq} are the $d-q$ frame inductance of the generator, Φ_{mag} is expressed as modulation flux linkage and J represents the cumulative inertia of the WT system. The electromagnetic torque of the PMVG is as follows:

$$T_{elec} = \frac{3}{2} P_n i_{sq} \Phi_{mag}. \tag{5}$$

3. The Proposed Rotor Speed Control Design

This section describes the RMAC design and its stability analysis. First, according to the system dynamics, the reference model is designed. Then, the proposed RMAC-based speed control law is created. It consists of a stabilizing feedback term and an adaptive term.

3.1. Reference Model for the Rotor Speed Control Design

The conventional model reference adaptive control is presented in [28], and the reference model rotor speed ω_{mr} is directly compared with the actual rotor speed ω_m. Likewise, in [29], the output of the reference model is compared to the electrical speed error, which is obtained from the real and desired rotor speeds. Based on the sampling period, the desired speed is changing. However, this study calculates the desired speed accurately from the RNN controller according to the obtained wind speed. Therefore, it gives a better dynamic performance, and the generator can extract the maximum power under wind speed variation. Figure 4 shows the block diagram of the proposed RMAC and RNN-based wind speed estimation controller. In (4), the rotor speed is in the form of a first-order derivative. Therefore, the reference model is also taken in the same way as follows [29]:

$$\dot{\omega}_{mr} + \lambda_{mr}\omega_{mr} = 0. \tag{6}$$

where $\lambda_{mr} > 0$ is a constant term, and ω_{mr} is the reference model output. In addition, the reference model output has following the exponential decay form:

$$\omega_{mr} = ce^{\lambda_{mr}t}, \tag{7}$$

where $c > 0$. The error dynamics are created by using the error vector $e = [e_1, e_2]$ as follows:

$$\begin{cases} e_1 = & \int_0^t e_w dt = \int_0^t e_2 dt, \\ \dot{e}_1 = & e_2, \\ \dot{e}_2 = & R_1 i_{sq} - R_2\omega_m - R_3 T_L + \lambda_{mr}\omega_{mr}. \end{cases} \tag{8}$$

where $R_1 = \dfrac{3}{2J} P_n \Phi_{mag}$, $R_2 = \frac{B}{J}$, $R_3 = P_n$, and $e_2 = \omega_e - \omega_{mr}$. The state variables are i_{sd}, i_{sq}, and ω_m, while R_1, R_2 and R_3 are unknown in (8). The tracking error is defined as follows:

$$\varphi = \mu e_1 + e_2. \tag{9}$$

where $\mu > 0$ is constant. Using the lemma 1 from [29], we can derive that

$$\Omega^* = -\frac{1}{R_1}\left[\mu - R_2, \lambda_{mr} - \mu, \mu\omega_d + R_3 T_L\right]^T. \tag{10}$$

Here, the load torque T_L and parameters $R_1, R_2, R_3, \mu, \lambda_{mr}$ and ω_d are unknown, and their differentiation is zero. Therefore, the considered parameters are constant.

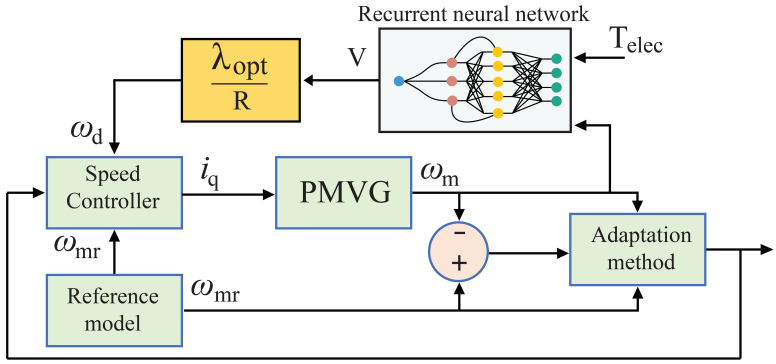

Figure 4. Block diagram of the proposed RMAC and the RNN-based wind estimation model.

3.2. Reference Model Adaptive Control Design for the Speed Control

This subsection describes the proposed RMAC design, which includes stabilizing feedback control and an adaptive compensatory control term. Then, using the Lyapunov technique, Theorem 1 proves the asymptotic stability of the closed-loop system.

Theorem 1. *If the PMVG parameters are unknown, the reference q-axis current i_q can be expressed as a combination of a stabilizing feedback control term ($k\varphi$) and an adaptive compensating control term ($\hat{\Omega}^T f$) , as shown below [29].*

$$i_q = -k\varphi + \hat{\Omega}^T f. \tag{11}$$

where $(\hat{\Omega}^T)$ is the adaptive compensating control term, $(-k\varphi)$ is the stabilizing feedback control term and the $f = [f_1,\ f_2,\ f_3]^T$. The updating law for RMAC is as follows:

$$\dot{\hat{\Omega}} = -\Theta^{-1} f \varphi, \tag{12}$$

where the adaptation gain $\Theta = diag(\Theta_1, \Theta_2, \Theta_3) > 0$.

Proof. The Lyapunov function is defined as follows:

$$V = \frac{\varphi^2 + R_1 \varrho^T \Theta \varrho}{2}, \tag{13}$$

where $\varrho = \Omega^* - \hat{\Omega}$. Then, the time derivative of (14) is given by

$$\frac{dV}{dt} = \frac{1}{2}\left[2\varphi\frac{d\varphi}{dt} + 2R_1\varrho^T\Theta\frac{d\varrho}{dt}\right], \tag{14}$$

$$\dot{V} = \varphi(\mu\dot{e_1} + \dot{e_2}) + R_1\varrho^T f\varphi \tag{15}$$

By using the Lemma 1 in [29], we can verify that

$$\dot{V} = -R_1 k\varphi^2 \leq 0 \tag{16}$$

which implies that $\dot{V} \leq 0$, as shown in (16), $V(t)$ is non-increasing and has an upper bound ($V(t) \leq V(0)$). Hence, we can conclude that the proposed control scheme guarantees the stable performance under Lyapunov stability theory. □

From (9), the transfer function of the tracking error is expressed as follows:

$$G(s) = \frac{1}{s+\mu} \tag{17}$$

From (11), the estimate term $\hat{\Omega}$ can be written as follows:

$$\hat{\Omega} = \begin{bmatrix} \hat{\Omega}_1 \\ \hat{\Omega}_2 \\ \hat{\Omega}_3 \end{bmatrix} = -\left[\int_0^t \frac{\varphi \omega_m}{\Theta_1} dt \quad \int_0^t \frac{\varphi \omega_{mr}}{\Theta_2} dt \quad \int_0^t \frac{\varphi}{\Theta_3} dt \right]^T \tag{18}$$

From (18), the update law of (11) can be written as:

$$\hat{\Omega}^T f = -\left[\omega_m \int_0^t \frac{\varphi \omega_m}{\Theta_1} dt + \omega_{mr} \int_0^t \frac{\varphi \omega_{mr}}{\Theta_2} dt + \int_0^t \frac{\varphi}{\Theta_3} dt \right] \tag{19}$$

where $f = [f_1,\ f_2,\ f_3]^T = [\omega_m,\ \omega_{mr},\ 1]^T$

4. The Proposed RNN for Wind Speed Estimation

The neural networks can learn and process data in parallel to achieve output values. Furthermore, the universal NN approximation theorem states that NN can accurately approximate any nonlinear behavior with single or several hidden layers [30]. In this respect, an RNN is a deep learning network topology presented to improve the network performance on current and future inputs by using knowledge from the past. In addition, RNNs are distinct in that they have a hidden state and loops, which enables the network to retain previous data in a hidden state and operate on sequences. The topology of the RNN scheme is as illustrated in Figure 5. In addition, the RNN outperforms other frequently used NNs in speed and efficiency, making it ideal for real-time control and identification applications. Furthermore, by picking adequate input signals, the RNN detects the wind speed reference accurately. The RNN input and output can be written as:

$$\begin{cases} \mathcal{I}_j = & \mathcal{W}_j O_j(k-1) + \sum_{j=1}^{n} \Xi_{ij} S_i \\ \mathcal{O}_j = & \dfrac{exp(\mathcal{I}_j)}{exp(\mathcal{I}_j) + exp(-\mathcal{I}_j)} \end{cases} \tag{20}$$

where the hidden layer input and output denote $\mathcal{I}_j$ and $\mathcal{O}_j$ $(j = 1, 2, \ldots n)$, W_j and Ξ_{ij} denote the recurrent weight and the connecting weight, respectively, and k denotes the sampling instant.

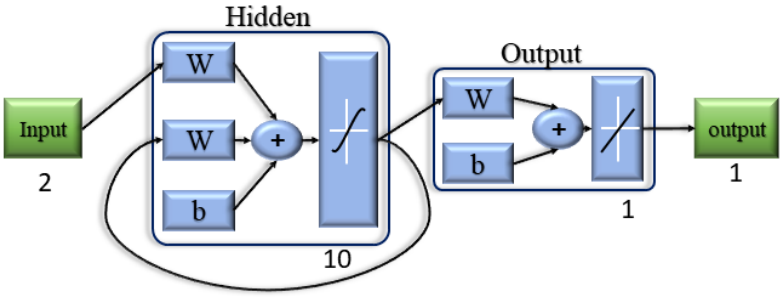

Figure 5. Topology of the recurrent neural networ.

Based on [31], the wind speed is measured using wind speed sensors. However, in this study, the wind speed V is measured using the generator speed ω_m and the electromagnetic

torque T_{elec}. Therefore, the RNN inputs are ω_m and T_{elec} and the output is V. In the input layer, the inputs are $d_1 = \omega_m$ and $d_2 = T_{elec}$ and the following is output:

$$\mathcal{S}_i = f(d_i) = \frac{exp(d_i) - exp(-d_i)}{exp(d_i) + exp(-d_i)} \tag{21}$$

where d_i $(i = 1, 2)$ denotes the i-th input of the input layer, $\mathcal{S}_i$ represents the i-th ouput of the input layer, and a symmetrical hyperbolic tangent sigmoid function is defined as $f(d_i)$. A single neuron in the output layer calculates the wind speed V as the weighted sum of all hidden layer output signals. Therefore, the final output of the estimated wind speed can be written as follows :

$$V = \sum_{j=1}^{n} \mathcal{W}_{j1} \mathcal{O}_j. \tag{22}$$

On the other hand, an RNN is trained using the numerical model of the PMVG-based WECS. In addition, the generator speed and torque are used as inputs, and the output is the wind speed. These are calculated within the range of 2–4 m/s and with the respective rotor speed and generator torque with an increment of 0.25 m/s. Moreover, the calculated numerical data are considered as training data. After training, validating, and testing, the mean square error is reached not more than 400 iterations, as shown in Figure 6. Therefore, the proposed NN can provide the estimated wind speed output with very minimum error value.

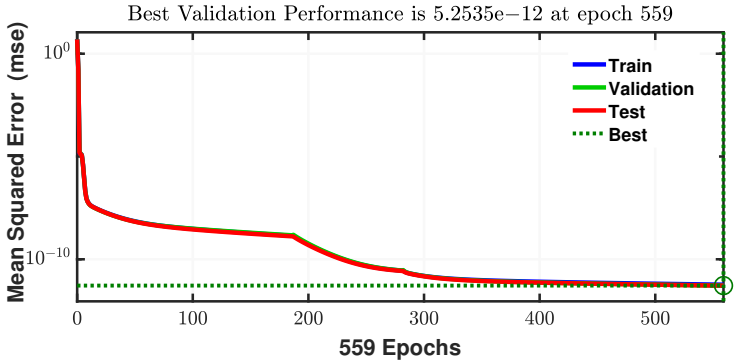

Figure 6. Neural network training performance.

5. Pitch Angle Controller

When the wind speed increases or power decreases, the rotor speed rises beyond the rated speed. In such a situation, the pitch angle regulation is activated to keep the rotor speed at its rated speed to maximize the output power, as shown in Figure 7. Then, the optimum pitch angle is used in the rotor-side control method, which can operate between lower and higher rotor speeds. Therefore, the rotor speed and pitch angle control are employed separately to sustain continuous power generation in WECS for balancing the input/output power [32].

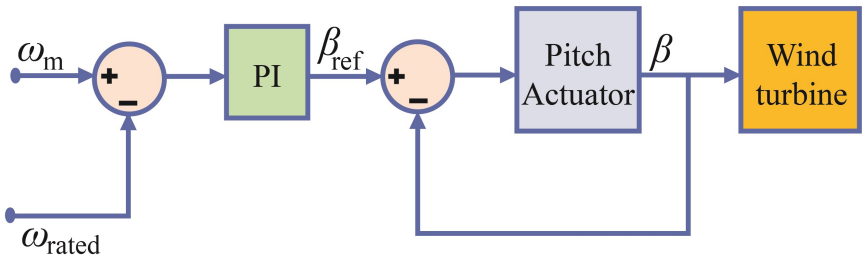

Figure 7. Pitch angle controller design for WT.

6. Simulation and Experimentation Results

6.1. Simulation Verification and Discussion

The PMVG-based variable speed WECS simulation is carried out to validate the efficiency of the proposed control method. Table 1 displays the PMVG-based WECS parameters, as similar in [27]. In this study, the PMVG-based WECS is investigated under the following three cases:

1. A random wind speed under region II;
2. A random wind speed under regions II and III;
3. A real wind speed is measured at the location of Gunsan, South Korea.

To do this, the constant λ_{mr} in the reference model (6) is set as 1000, and the c value in (7) is set as 0.25. The gain k in the feedback control (11) is 0.51. In addition, the proposed RMAC system dynamic performance is compared using proportional integral (PI) and optimal torque control (OTC) [33,34] methods.

Figure 8 shows the step wind speed and the corresponding wind speed estimated by the RNN for each step variation. It shows that there is a small time transient in the wind speed estimation with no oscillations before settling.

Table 1. Parameters of PMVG-based WECS [27].

Parameter	Symbol	Value
Rated power	P_{wt}	5 kW
Air density	ρ	1.225 kg/m^3
Radius	R	2.82 m
Moment of inertia	J	0.188 kg·m^2
Resistance	R_s	0.44 Ω
d-q inductanc of generator	L_{sd}, L_{sq}	17.5 mH
No. of poles	P_n	20
Flux density	Φ_{mag}	0.4459 Wb

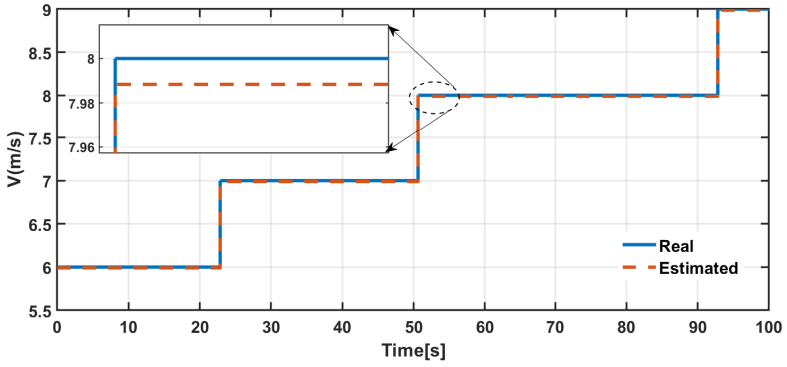

Figure 8. Real and estimated wind speeds.

6.1.1. Case I: A Random Wind Speed under the Region II

In this case, wind speed is below 9 m/s and β is zero. Figure 9 shows the comparative simulation results of the PI, OTC controllers and the proposed control method, respectively. The region II random wind speed is shown in Figure 9a, with an upper limit of 9 m/s and a lower limit of 6.3 m/s. Moreover, the rotor speed tracking performance is illustrated in Figure 9b, with the different control methods. From this, it is evident that the rotor speed tracks the optimal rate much more rapidly and efficiently when comparing the proposed control method to the other control methods in terms of overshoot and settling time. From Figure 9c, we can confirm that the proposed control method can recover C_p to $C_{p_{max}}$ very quickly compared to the PI and OTC methods. In addition, for varying wind speeds, the rotor speed tracks the reference speed to maintain a consistent power coefficient. As a result, the MPPT under region II yields the best value of $C_p = 0.4412$. Moreover, as seen in

Figure 10, we can see the TSR (λ) can be smoothly maintained around the excellent value (6.912) under the proposed control scheme.

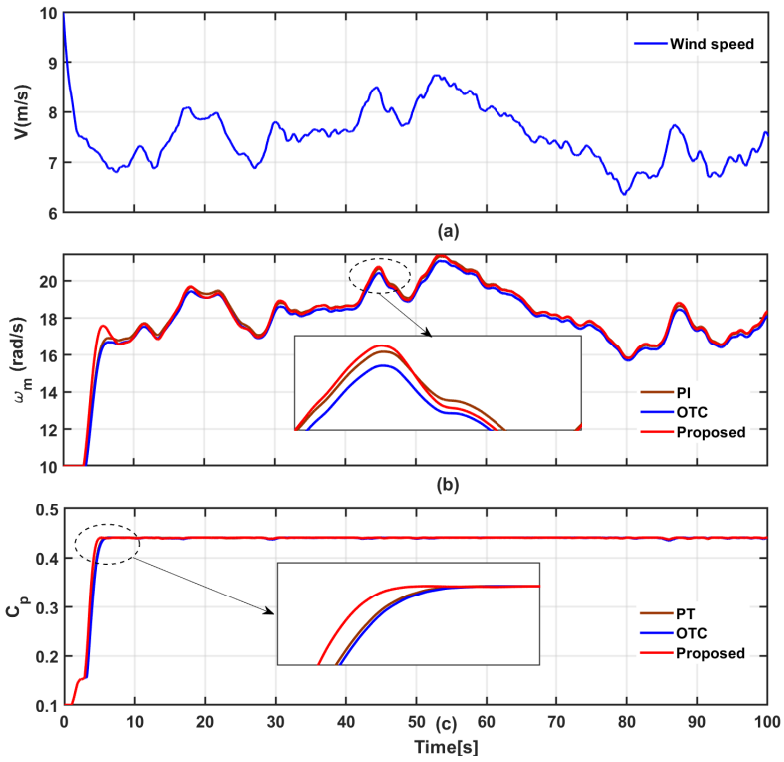

Figure 9. Simulation results for PMVG-based WECS under the case I with region II wind speed: (**a**) Random wind speed. (**b**) Rotor speed. (**c**) Power coefficient.

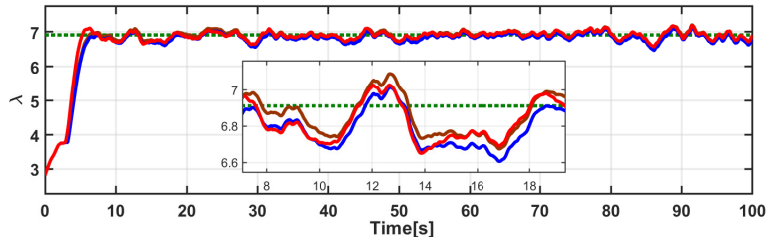

Figure 10. Lambda for region II.

6.1.2. Case II: A Random Wind Speed under the Region II and III

In this case, the random wind speed changes across regions II and III, with wind speeds ranging from 7.1 to 10 m/s. As mentioned earlier, when the wind speed hits 9 m/s, the PMVG rated rotor speed of 22.3 rad/s is reached. Thus, when the wind speed exceeds 9 m/s, the pitch control shifts the WT blades to the pitch angle that minimizes mechanical stress. Accordingly, the λ and C_p values are also lowered. When the wind speed drops below 9 m/s, the MPPT kicks in to provide rotor speed control. In detail, Figure 11 provides the dynamic performance of the simulation results of the PI, OTC controllers and the proposed control method, respectively. Following that, Figure 11a shows the variable wind speed. At the same time, the rotor speed is presented in Figure 11b.

From this, it can be observed that pitch angle control is activated when the wind speed exceeds 9 m/s; then, the C_p and λ values will be reduced to maintain the rotor speed below the rated speed of 22.3 rad/s. Thus, the generator power also reduced correspondingly. The enlarged figure inside Figure 11b clearly confirms that the proposed controller technique effectively achieves the MPPT target compared to the PI and OTC controllers. The corresponding power and C_p are displayed in Figure 11c,d, respectively.

The corresponding λ and β values are illustrated in Figure 12a and Figure 12b, respectively.

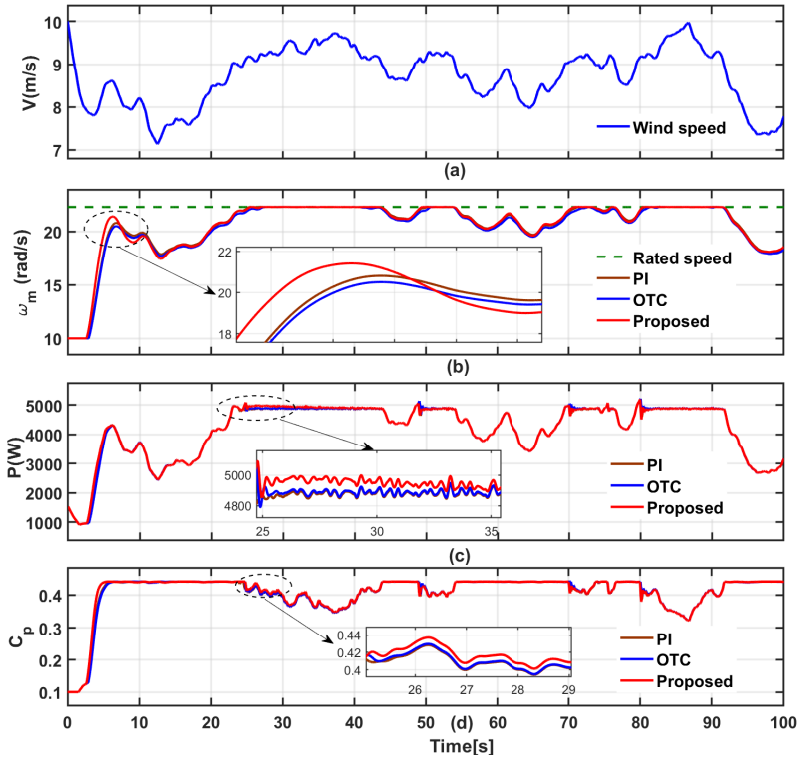

Figure 11. Simulation results for PMVG-based WECS under the case II with region II and region III wind speed: (**a**) Random wind speed. (**b**) Rotor speed. (**c**) Output power. (**d**) Power coefficient.

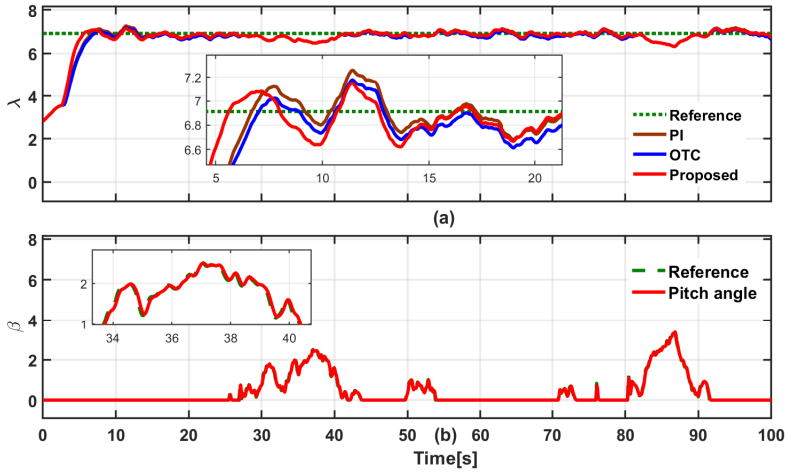

Figure 12. Results for the case II with wind speed of region II and III: (**a**) Tip speed ratio λ. (**b**) Pitch angle β.

6.1.3. Case III: Real Wind Speed

In this case, actual wind speed data for 10 min are gathered from the place of Gunsan in South Korea. It is measured by using an anemometer, which is called point wind speed. However, point wind speed cannot be used directly, so we estimate the effective wind speed using the Newton Raphson equation [35], as shown in Figure 13. For simulation, the estimated wind speed duration is 100 s ranging from 5 to 13.7 m/s. Furthermore, Figure 14 shows the comparison of the dynamic performance of PMVG for real wind speed. First, the real wind speed is clearly shown in Figure 14a. From Figure 14b, it is evident

that the proposed RMAC-based speed tracking control responds faster than the existing control methods.

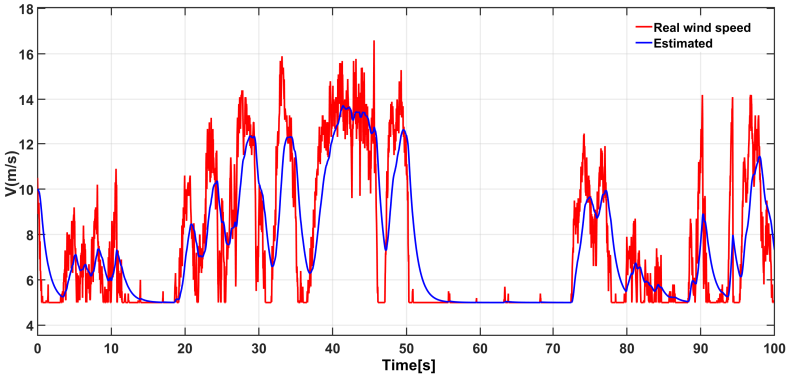

Figure 13. Estimated real wind speed profile.

At this time, the C_p value is increased because the rotor speed effectively tracks the reference speed, as seen in Figure 14c. In addition, as illustrated in Figure 14d, the WT output power is more elevated than the PI and OTC controllers. The corresponding λ and β values are given in Figure 15. From this result, we can confirm that the proposed method's average generator output power for a specific period (100 s) is 0.5489% greater than the PI controller and 1.973% higher than the OTC control method. In addition, dynamic responses within the graphs are highlighted during low and high wind speeds. It has been shown that speed tracks form smoothly when all control methods are used. However, for the proposed control method, the generator speed is accelerated or slowed down very quickly during the MPPT operation under the actual wind speed variation compared to the PI and OTC control methods. Hence, it is worth concluding that the proposed control scheme effectively tracks the MPPT reference under varying wind conditions.

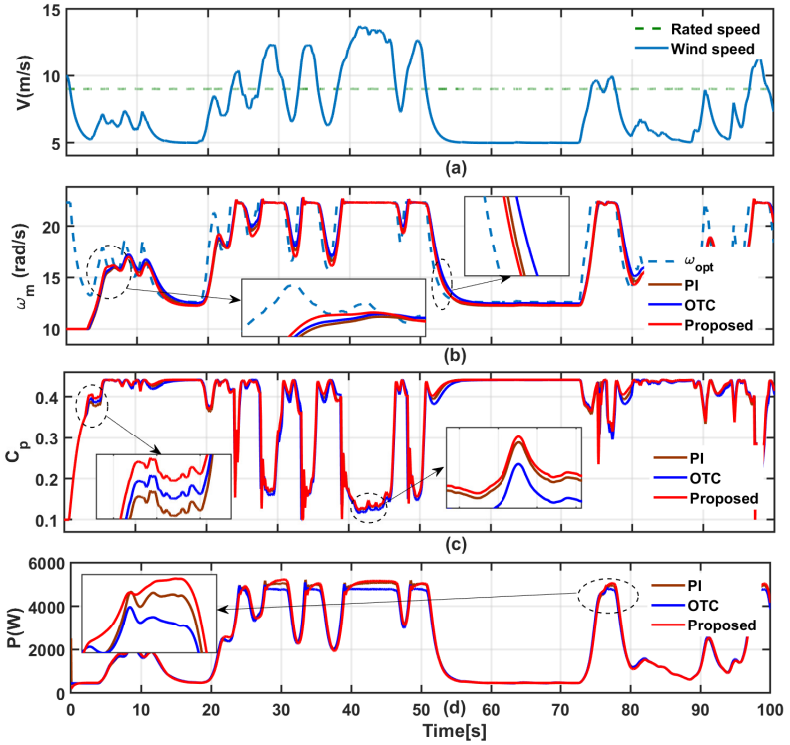

Figure 14. Results for the case III with real wind speed: (**a**) Real wind speed. (**b**) Rotor speed. (**c**) Power coefficient. (**d**) Output power.

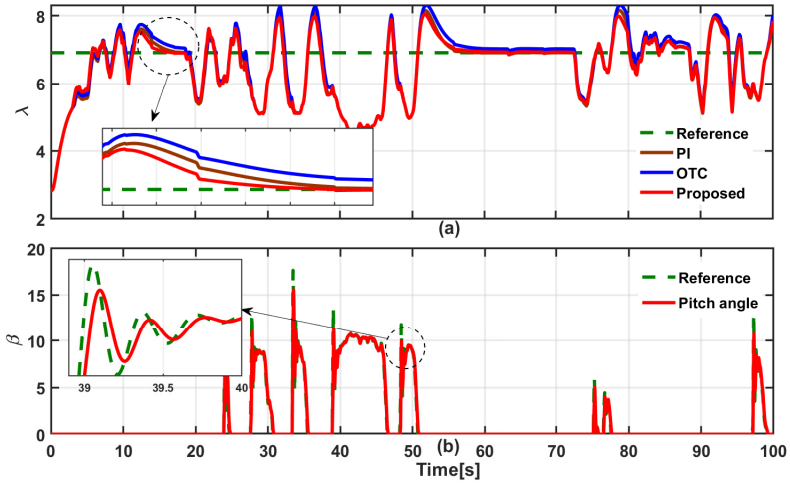

Figure 15. Results for case III with real wind speed. (**a**) Tip speed ratio λ. (**b**) Pitch angle β.

Finally, the rotor speed tracking performance and quantitative analysis for power extraction are given in Table 2. These findings proved that the proposed RMAC for rotor speed tracking control outperforms the other conventional methods. Moreover, the electrical power extraction also significantly improved. Using the proposed controller, we may gain 2.35% and 0.38% more than the PI and OTC controllers in region II. We may achieve 1.01% and 0.23% greater than the PI and OTC controllers in regions II and III. We can achieve 1.75% and 1.16% higher than the PI and OTC controllers in real wind speed conditions.

Table 2. PMVG rotor speed tracking performance and electrical power efficiency analysis from the simulation results.

Regions	Control Methods	Tracking Efficiency (%)	Electrical Power Efficiency (%)
II	PI	94.25	84.82
	OTC	95.24	85.71
	Proposed	95.60	86.04
II and III	PI	93.75	84.37
	OTC	94.48	85.03
	Proposed	94.70	85.23
Under real wind speed	PI	92.58	83.32
	OTC	93.12	83.80
	Proposed	94.21	84.78

6.2. Experimental Verification and Discussion

The experimental setup of the PMVG-based WECS is shown in the Figure 16. A Sinamics-S120 power controller controls a Siemens induction motor that emulates a wind turbine model. A 5 kW PMVG coupled with an induction motor and a three-phase back-to-back converter is used to rectify the generator AC voltage. The Texas Instruments TMS320F28335 DSP board with a 10 kHz sampling frequency is used to implement the control methods, and the easy DSP platform is used to monitor the response of the system. In addition, to test the efficiency of the proposed control strategy, it is compared to the OTC method, which is commonly used in industrial purposes.

The dynamic behaviors of the PMVG-based WECS under the proposed control scheme are demonstrated in Figure 17. First, the real wind speed given in Figure 17a. From Figure 17b, we can affirm that the proposed control method can offer good rotor speed tracking performance under real wind speed fluctuations. Following the MPPT operation,

when the wind speed is below the rated speed (region II), the power coefficient is maintained at its maximum value $C_p = 0.441$, and the blades are at their ideal angle $\theta = 0^o$. Conversely, if the wind speed exceeds the rated speed (region III) of the turbine, the WECS switches to pitch angle control its lowered the power coefficient, as illustrated in Figure 17c. From Figure 17d, we can confirm that the proposed control method effectively operates the WECS under MPPT conditions. In addition, the rise in pitch angle at high wind speeds is displayed in Figure 18a. From Figure 18b, it is evident that the proposed control scheme enhances the stable MPE for the real varying wind conditions. Furthermore, the negative sign indicates that the generator output power is transformed to the grid. From the rigorous analysis of the simulation and experimental results, we conclude that the proposed control method exhibits the fast dynamic response and stable power extraction capability over existing control methods.

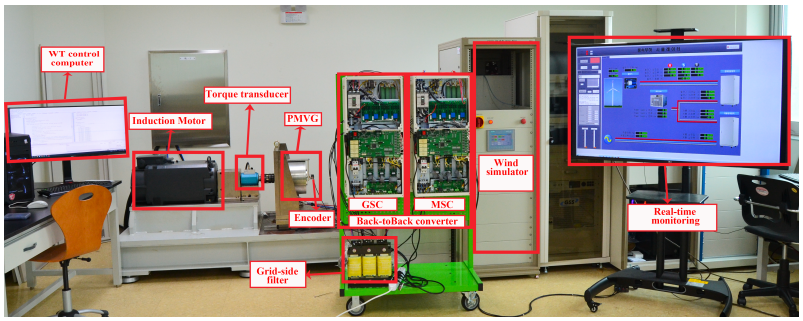

Figure 16. Hardware of the experimental setup.

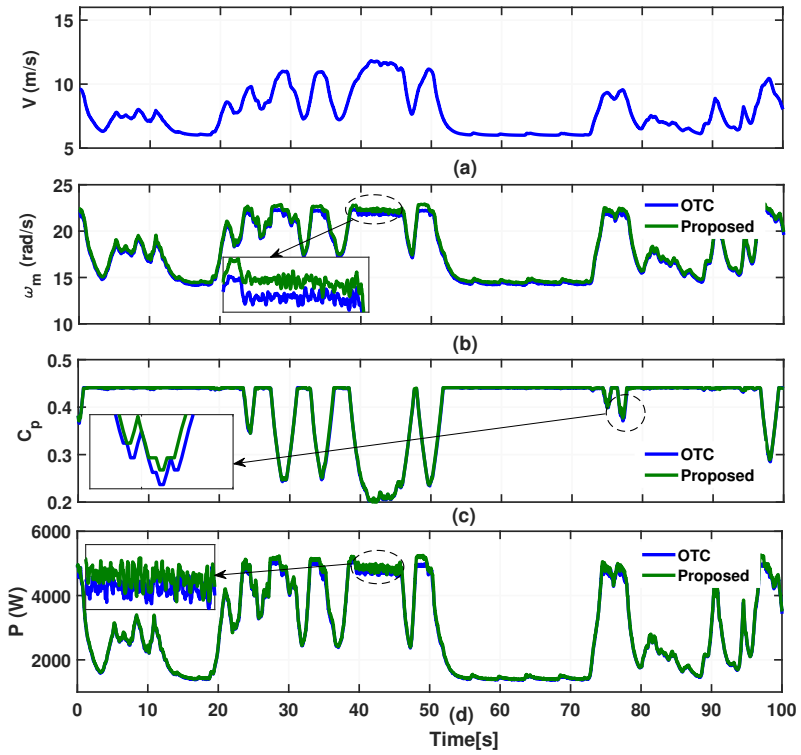

Figure 17. Experimental results for real wind speed: (**a**) Real wind speed. (**b**) Rotor speed. (**c**) Power coefficient. (**d**) Output power.

Finally, an overview of rotor speed tracking performance and electrical power extraction efficiency are compared and given in Table 3. These findings proved that the proposed RMAC for rotor speed tracking and electrical power extraction outperforms the OTC method. Furthermore, using the proposed controller may acquire 2.56% more electrical power than the OTC controller.

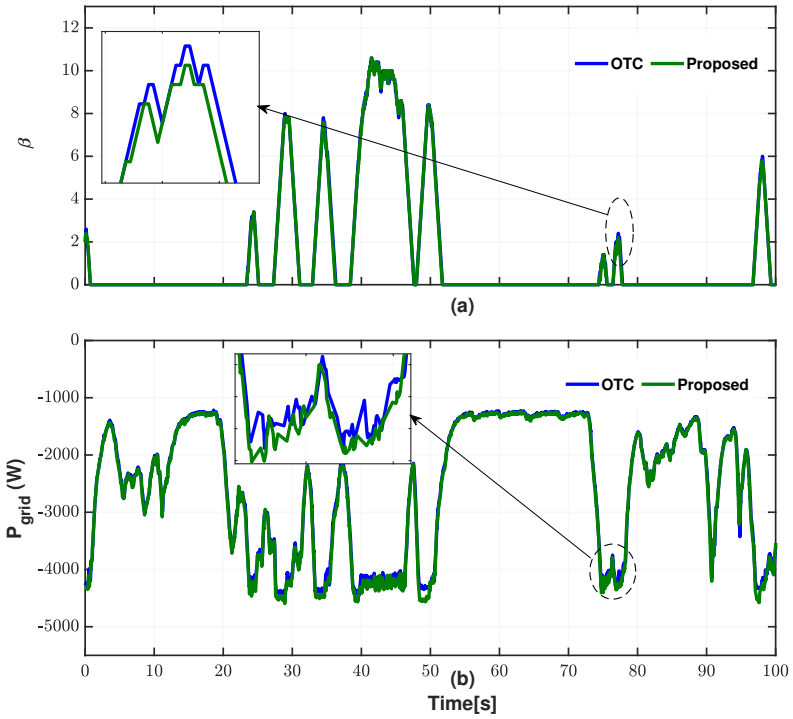

Figure 18. Experimental results for real wind speed: (**a**) Beta β. (**b**) Grid output power.

Table 3. PMVG rotor speed tracking performance analysis and electrical power efficiency from the experimental results.

Control Methods	Tracking Efficiency (%)	Electrical Power Efficiency (%)
OTC	94.24	83.01
Proposed	94.60	85.14

7. Conclusions

In this study, an RMAC has been investigated for a DD PMVG-based WECS under real wind speed conditions. To do this, first, RMAC-based rotor speed tracking control has been presented to track a reference model that guarantees the expected exponential decay of rotor speed error trajectory. Next, an RNN-based training model has been presented to estimate the actual wind speed without using the wind speed measuring sensor. In addition, the pitch angle control has been presented to operate the rotor speed within the allowable operating range, ensuring the stable power production of the WECS. We have shown that the proposed control asymptotic stability has been guaranteed using Lyapunov theory. Finally, the proposed control system has demonstrated its effectiveness through some simulations and experimentation using a prototype of 5 kW DD PMVG-based WECS. In addition, the comparative results have verified the superiority of the proposed control over the existing control methods.

Author Contributions: Conceptualization, A.A.Y.; methodology, A.A.Y.; validation, A.A.Y., Y.H.J. and S.R.L.; formal analysis, Y.H.J. and S.R.L.; writing—original draft preparation, A.A.Y.; writing—review and editing, A.A.Y., Y.H.J. and S.R.L.; supervision, Y.H.J.; funding acquisition, Y.H.J. All authors have read and agreed to the published version of the manuscript.

Funding: This work was partially supported by the Basic Science Research Program through the National Research Foundation of Korea (NRF) funded by the Ministry of Education (NRF-2016R1A6A1A03013567, NRF-2021R1A2B5B01001484).

Institutional Review Board Statement: Not applicable.

Informed Consent Statement: Not applicable.

Conflicts of Interest: The authors declare no conflict of interest.

References

1. Guerroudj, C.; Saou, R.; Boulayoune, A.; Zaïm, M.E.h.; Moreau, L. Performance analysis of Vernier slotted doubly salient permanent magnet generator for wind power. *Int. J. Hydrogen Energy* **2017**, *42*, 8744–8755. [CrossRef]
2. Tiwari, R.; Padmanaban, S.; Neelakandan, R.B. Coordinated control strategies for a permanent magnet synchronous generator based wind energy conversion system. *Energies* **2017**, *10*, 1493. [CrossRef]
3. Tlali, P.; Wang, R.J.; Gerber, S. Comparison of PM vernier and conventional synchronous 15 kW wind generators. In Proceedings of the IEEE 2018 XIII International Conference on Electrical Machines (ICEM), Alexandroupoli, Greece, 3–6 September 2018; pp. 2065–2071.
4. Toba, A.; Lipo, T.A. Generic torque-maximizing design methodology of surface permanent-magnet vernier machine. *IEEE Trans. Ind. Appl.* **2000**, *36*, 1539–1546.
5. Kim, B. Design of a direct drive permanent magnet Vernier generator for a wind turbine system. In Proceedings of the 2018 IEEE Energy Conversion Congress and Exposition (ECCE), Portland, OR, USA, 23–27 September 2018; pp. 4275–4282.
6. Li, J.; Chau, K.; Jiang, J.; Liu, C.; Li, W. A new efficient permanent-magnet vernier machine for wind power generation. *IEEE Trans. Magn.* **2010**, *46*, 1475–1478. [CrossRef]
7. Jang, D.; Chang, J. Influences of winding MMF harmonics on torque characteristics in surface-mounted permanent magnet vernier machines. *Energies* **2017**, *10*, 580. [CrossRef]
8. Kim, B. Design method of a direct-drive permanent magnet vernier generator for a wind turbine system. *IEEE Trans. Ind. Appl.* **2019**, *55*, 4665–4675. [CrossRef]
9. Labuschagne, C.; Kamper, M. Permanent magnet vernier generator design for a small-scale passive wind generator system. In Proceedings of the 2021 IEEE International Electric Machines & Drives Conference (IEMDC), Hartford, CT, USA, 17–20 May 2021; pp. 1–7.
10. Labuschagne, C.; Kamper, M. Performance and cost comparison of conventionaland vernier PM wind generators for small-scale uncontrolled passive wind energy systems. In Proceedings of the 2021 IEEE Energy Conversion Congress and Exposition (ECCE), Vancouver, BC, Canada, 10–14 October 2021; pp. 4591–4597.
11. Tang, X.; Yin, M.; Shen, C.; Xu, Y.; Dong, Z.Y.; Zou, Y. Active power control of wind turbine generators via coordinated rotor speed and pitch angle regulation. *IEEE Trans. Sustain. Energy* **2018**, *10*, 822–832. [CrossRef]
12. Munteanu, I.; Cutululis, N.A.; Bratcu, A.I.; Ceangă, E. Optimization of variable speed wind power systems based on a LQG approach. *Control Eng. Pract.* **2005**, *13*, 903–912. [CrossRef]
13. Dash, P.; Patnaik, R. Adaptive second order sliding mode control of doubly fed induction generator in wind energy conversion system. *J. Renew. Sustain. Energy* **2014**, *6*, 053143. [CrossRef]
14. Majout, B.; Bossoufi, B.; Bouderbala, M.; Masud, M.; Al-Amri, J.F.; Taoussi, M.; El Mahfoud, M.; Motahhir, S.; Karim, M. Improvement of PMSG-Based Wind Energy Conversion System Using Developed Sliding Mode Control. *Energies* **2022**, *15*, 1625. [CrossRef]
15. Mohamed, A.Z.; Eskander, M.N.; Ghali, F.A. Fuzzy logic control based maximum power tracking of a wind energy system. *Renew. Energy* **2001**, *23*, 235–245. [CrossRef]
16. Li, L.; Ren, Y.; Alsumiri, M.; Brindley, J.; Jiang, L. Maximum power point tracking of wind turbine based on optimal power curve detection under variable wind speed. In Proceedings of the International Conference on Renewable Power Generation (RPG 2015), Beijing, China, 17–18 October 2015; pp. 1–6. [CrossRef]
17. Vu, V.P.; Ngo, V.T.; Do, V.D.; Truong, D.N.; Huynh, T.T.; Do, T.D. Robust MPPT observer-based control system for wind energy conversion system with uncertainties and disturbance. *IEEE Access* **2021**, *9*, 96466–96477. [CrossRef]
18. Sitharthan, R.; Karthikeyan, M.; Sundar, D.S.; Rajasekaran, S. Adaptive hybrid intelligent MPPT controller to approximate effectual wind speed and optimal rotor speed of variable speed wind turbine. *ISA Trans.* **2020**, *96*, 479–489. [CrossRef] [PubMed]
19. Putri, R.I.; Pujiantara, M.; Priyadi, A.; Ise, T.; Purnomo, M.H. Maximum power extraction improvement using sensorless controller based on adaptive perturb and observe algorithm for PMSG wind turbine application. *IET Electr. Power Appl.* **2018**, *12*, 455–462. [CrossRef]
20. Buettner, M.A.; Monzen, N.; Hackl, C.M. Artificial neural network based optimal feedforward torque control of interior permanent magnet synchronous machines: A feasibility study and comparison with the state-of-the-art. *Energies* **2022**, *15*, 1838. [CrossRef]
21. Yin, X.; Jiang, Z.; Pan, L. Recurrent neural network based adaptive integral sliding mode power maximization control for wind power systems. *Renew. Energy* **2020**, *145*, 1149–1157. [CrossRef]
22. Dahbi, A.; Nait-Said, N.; Nait-Said, M.S. A novel combined MPPT-pitch angle control for wide range variable speed wind turbine based on neural network. *Int. J. Hydrogen Energy* **2016**, *41*, 9427–9442. [CrossRef]
23. Alzayed, M.; Chaoui, H.; Farajpour, Y. Maximum power tracking for a wind energy conversion system using cascade-forward neural networks. *IEEE Trans. Sustain. Energy* **2021**, *12*, 2367–2377. [CrossRef]

24. George, T.; Jayaprakash, P.; Subramaniam, U.; Almakhles, D.J. Frame-angle controlled wavelet modulated inverter and self-recurrent wavelet neural network-based maximum power point tracking for wind energy conversion system. *IEEE Access* **2020**, *8*, 171373–171386. [CrossRef]
25. Wu, F.; Jing, R.; Zhang, X.P.; Wang, F.; Bao, Y. A combined method of improved grey BP neural network and MEEMD-ARIMA for day-ahead wave energy forecast. *IEEE Trans. Sustain. Energy* **2021**, *12*, 2404–2412. [CrossRef]
26. Slootweg, J.; De Haan, S.; Polinder, H.; Kling, W. General model for representing variable speed wind turbines in power system dynamics simulations. *IEEE Trans. Power Syst.* **2003**, *18*, 144–151. [CrossRef]
27. Joo, Y.H.; Antonysamy, R.; Ramasamy, T.; Lee, S.R. Stable maximum Power extraction and DC link voltage regulation for PMVG-based WECS. *IEEE Trans. Ind. Electron.* **2022**, 1. [CrossRef]
28. Guo, L.; Parsa, L. Model reference adaptive control of five-phase IPM motors based on neural network. *IEEE Trans. Ind. Electron.* **2011**, *59*, 1500–1508. [CrossRef]
29. Nguyen, A.T.; Rafaq, M.S.; Choi, H.H.; Jung, J.W. A model reference adaptive control based speed controller for a surface-mounted permanent magnet synchronous motor drive. *IEEE Trans. Ind. Electron.* **2018**, *65*, 9399–9409. [CrossRef]
30. Hornik, K. Approximation capabilities of multilayer feedforward networks. *Neural Netw.* **1991**, *4*, 251–257. [CrossRef]
31. Chen, J.; Yao, W.; Zhang, C.K.; Ren, Y.; Jiang, L. Design of robust MPPT controller for grid-connected PMSG-Based wind turbine via perturbation observation based nonlinear adaptive control. *Renew. Energy* **2019**, *134*, 478–495. [CrossRef]
32. Zhang, J.; Cheng, M.; Chen, Z.; Fu, X. Pitch angle control for variable speed wind turbines. In Proceedings of the 2008 Third International Conference on Electric Utility Deregulation and Restructuring and Power Technologies, Online, 6–9 April 2008, pp. 2691–2696.
33. Fazli, N.; Siahbalaee, J. Direct torque control of a wind energy conversion system with permanent magnet synchronous generator and matrix converter. In Proceedings of the IEEE 2017 8th Power Electronics, Drive Systems & Technologies Conference (PEDSTC), Mashhad, Iran, 14–16 February 2017; pp. 166–171.
34. Joo, Y. Integral sliding mode control for increasing maximum power extraction efficiency of variable-speed wind energy system. *Int. J. Electr. Power Energy Syst.* **2022**, *139*, 107958.
35. Rajendran, S.; Diaz, M.; Chavez, H.; Cruchaga, M.; Castillo, E. Terminal synergetic control for variable speed wind turbine using a two mass model. In Proceedings of the 2021 IEEE CHILEAN Conference on Electrical, Electronics Engineering, Information and Communication Technologies (CHILECON), Online, 6–9 December 2021; pp. 1–6.